Mechanical Systems and Signal Processing 107 (2018) 529–548

Contents lists available at ScienceDirect

Mechanical Systems and Signal Processing

journal homepage: www.elsevier.com/locate/ymssp

Identification of multiple leaks in pipeline: Linearized model, maximum likelihood, and super-resolution localization

Xun Wang *, Mohamed S. Ghidaoui

Department of Civil and Environmental Engineering, Hong Kong University of Science and Technology, Clear Water Bay, Hong Kong, China

ARTICLE INFO

Article history:
Received 19 June 2017
Received in revised form 21 December 2017
Accepted 29 January 2018

Keywords:
Leak detection
Defect detection
Transient wave
Maximum likelihood
Super-resolution
Cramér-Rao lower bound

ABSTRACT

This paper considers the problem of identifying multiple leaks in a water-filled pipeline based on inverse transient wave theory. The analytical solution to this problem involves nonlinear interaction terms between the various leaks. This paper shows analytically and numerically that these nonlinear terms are of the order of the leak sizes to the power two and; thus, negligible. As a result of this simplification, a maximum likelihood (ML) scheme that identifies leak locations and leak sizes separately is formulated and tested. It is found that the ML estimation scheme is highly efficient and robust with respect to noise. In addition, the ML method is a super-resolution leak localization scheme because its resolvable leak distance (approximately $0.15\lambda_{min}$, where λ_{min} is the minimum wavelength) is below the Nyquist-Shannon sampling theorem limit ($0.5\lambda_{min}$). Moreover, the Cramér-Rao lower bound (CRLB) is derived and used to show the efficiency of the ML scheme estimates. The variance of the ML estimator approximates the CRLB proving that the ML scheme belongs to class of best unbiased estimator of leak localization methods.

1. Introduction

Leaks in water supply pipelines is a problem of increasing interest due to their associated financial cost from the wastage of resources as well as their ability to act as entry points for contaminants into the treated water system. Various leak detection methods have been developed in the past decades with acoustic analysis as one of the more popular techniques. The fact that 40% of water is lost from pipes around the world is a clear testimony that current methods are far from satisfactory and there is an urgent need to fill this gap. As a result, recent researches have focused on transient-based leak detection methods (TBDMs). TBDMs utilize the hydraulics of transient flows to detect leaks in the pipeline, e.g., Refs. [1–18]. The tenet of TBDM is that leaks can be identified by injecting perturbations into a pipeline and measuring and analysing the system response (e.g., pressure head) at specified location(s). The reason that such methods are expected to work is that a leak in a pipeline system is known to result in an increased damping of the transient pressure and acts as "reflector" to the transient wave [19]. Many TBDMs have been developed by researchers and applied to water piping systems. The class of TBDM that uses the reflective property of a leak is called transient reflection based method (TRM) [2,20–23]. Another class that uses the damping property of leak is called transient damping based Method (TDM) [5]. A third class of TBDM uses both damping and reflective properties and can be found in Refs. [1,3,4,6–9,24–30]. Note that the TBDMs mainly concern transmission mains but they

* Corresponding author.
E-mail addresses: xunwang@ust.hk, xunwang00@gmail.com (X. Wang).

https://doi.org/10.1016/j.ymssp.2018.01.042
0888-3270/

Nomenclature

q	discharge oscillation
h	head oscillation
x^L	leak location
z^L	pipe elevation at leak
s^L	leak size
Q_0^L, H_0^L	steady-state discharge and head of leak
x^M	sensor coordinate
$\Delta\mathbf{h}$	head difference
$\mathbf{n}$	measurement noise
a	wave speed
A	area of pipeline
l	pipe length
g	gravitational acceleration
Z	characteristic impedance
R	frictional resistance
F	Darcy-Weisbach friction factor
μ	propagation function
ω	angular frequency
ω_{th}	fundamental frequency
λ_{min}	minimum wavelength
M	sensor number
N	leak number
J	frequency number
T	sample size
σ^2	variance of noise
$\log L$	log-likelihood function

Superscripts

L	leak
U	upstream node
D	downstream node
NL	no leak
SL	single leak
M	measurement
H	conjugate transpose

Acronyms

CRLB	Cramér-Rao lower bound
FIM	Fisher information matrix
FRF	frequency response function
MFP	matched-field processing
MFP(1)	MFP with one-leak model
ML	maximum likelihood
MLE	maximum likelihood estimate
MSE	mean square error
PDF	probability density function
RE	relative error
RMSE	root mean square error
SNR	signal-to-noise ratio

have been used in distribution mains [16]. Furthermore, TBDMs can detect not only leaks but also partial blockages, partially closed in-line valves, branches, etc [16,31–33]. However, there is no proof that these methods maximize signal-to-noise ratio (SNR) and there is no concerted effort in the literature to theoretically or analytically study the effect of noise on these existing methods using a probabilistic framework such as the maximum likelihood theory, although there have been attempts at evaluating the reliability of leak detection techniques with respect to noise [22]. Yet, ultimately, such methods would need to be applied in an often highly noisy environment due to traffic, turbulence, and mechanical devices.

Recently, the authors of this paper formulated a transient leak detection method based on a matched-field processing (MFP) method [34] and found that this approach is efficient, robust, accurate, provides a unique solution and maximizes SNR. MFP uses the full information in the measured signal, i.e., both the reflective and damping properties of leaks are incorporated. As a result, MFP uses all available frequencies, not just resonant frequencies. Therefore, there is no need to identify which frequencies are resonant frequencies. The fact that MFP uses all frequencies (i.e., all measured information) together with its ability to maximize SNR means that the MFP method provides precise localization estimates even in noisy environments. In fact, it is shown that the MFP method can locate and size leaks in the presence of (i) noise even for SNR as low as SNR $= -3.0$ dB and (ii) uncertainty in the wave speed. For the case of multiple leaks, MFP identifies separate leaks provided the distance between leaks is of the same order or larger than half the shortest probing wavelength. For cases where half of the shortest probing wavelength is large compared to the distance between the leaks, separation of individual leaks in the pipe is not possible. It is precisely this shortcoming of MFP that this paper addresses.

Following this introduction, a statement of the problem being addressed is given in Section 2. Then, a frequency-domain transient wave model for pipe systems is introduced in Section 3. The head difference due to the transient wave propagating from one end of the pipe to the other while passing by multiple leaks is analyzed. The head changes are then approximated by a linear combination of individual leak contributions, where the accuracy of this linear approximation is justified both mathematically and numerically. In Section 4, a maximum likelihood (ML) leak detection method is introduced and used to estimate both the positions and sizes of multiple leaks in a pipe system. In Section 5, the Cramér-Rao lower bound (CRLB) of leak locations and sizes is derived and it is shown that the ML approach maximizes SNR. Numerical simulations are introduced to illustrate the properties of the ML method in Section 6. Finally, some conclusions are drawn in Section 7.

2. Problem statement and goal of the paper

As stated in the introduction, although the MFP method introduced by the authors in Ref. [34] has several desirable attributes including efficiency, robustness, accuracy, uniqueness of solution and maximizing SNR, it is unable to separate multiple leaks when the shortest probing wavelength is large compared to the distance between the leaks. Numerical examples are introduced here to illustrate and clarify this deficiency in the MFP method proposed in Ref. [34]. The numerical test pipe system is shown in Fig. 1. A single, horizontal pipeline is connected by two reservoirs, whose coordinates are $x = x^U = 0$ and $x = x^D$ and their heads relative to pipeline centreline are respectively $H_1 = 25$ m and $H_2 = 20$ m. The pipe length is $l = 2$ km and the diameter is $D = 0.5$ m. The Darcy-Weisbach friction factor of the pipe is $F = 0.02$, the steady-state discharge is $Q_0 = 0.0306$ m^3/s (the subscript "0" indicates the steady-state condition), and the wave speed is assumed to be $a = 1200$ m/s. A valve is located at the downstream end of the pipe and two pressure sensors are situated upstream of the valve. An impulse wave is generated by the valve. The measurements from the sensors at $x^{M_1} = 1800$ m and $x^{M_2} = 1960$ m are used in the leak estimation process. First, two leaks at $x^{L_1} = 300$ m and $x^{L_2} = 700$ m with sizes $s^{L_1} = 1 \times 10^{-4}$ m^2 and $s^{L_2} = 1.2 \times 10^{-4}$ m^2 are considered. The leak size, flow and head relations are defined in the following section. Fig. 2(a) shows the estimate using the MFP with single-leak model: the cost function clearly shows two local maxima which correspond to the two leaks but the estimates of both leaks have slight errors (the two local maxima are at 295 m and 703 m). Then, two close leaks are considered, whose locations are $x^{L_1} = 400$ m and $x^{L_2} = 460$ m. Here, the frequencies $\omega = \{(1+\alpha)\omega_{th} : \alpha = 0, 0.02, 0.04, \ldots, 30\}$ are used, in which $\omega_{th} = a\pi/(2l) = 0.94$ Hz is the fundamental frequency (first resonant frequency). Therefore, the minimum wavelength is $\lambda_{min} = 258$ m. Fig. 2(b) shows that in this case the two close leaks, whose distance is approximately $0.23\lambda_{min}$, cannot be separately identified. In fact, Ref. [34] has shown that the minimum resolvable range that two leaks can be individually estimated is approximately $0.5\lambda_{min}$.

The main goal of this paper is to develop a method capable of identifying "close" multiple leaks using a super-resolution method. A super-resolution method should be able to identify multiple leaks even when the distance between them is less than half the shortest probing wavelength, and it should do so without sacrificing efficiency, robustness, accuracy, uniqueness, or maximum SNR attributes.

3. Linearized model of transient wave in pipeline with multiple leaks

This section describes a model for propagation of a transient wave in a pipeline. The main result and advantage of the proposed model is that the pressure head difference due to leakage can be approximated by a linear form, which is a super-

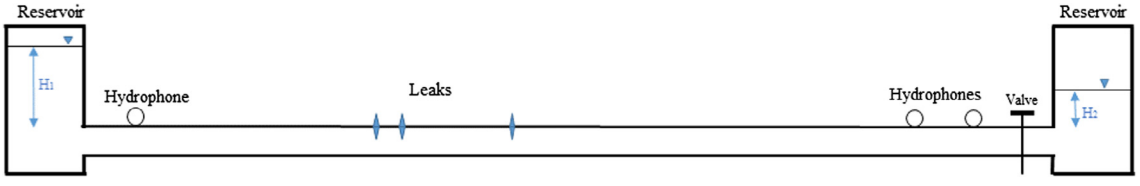

Fig. 1. Setup of the simulation experiment.

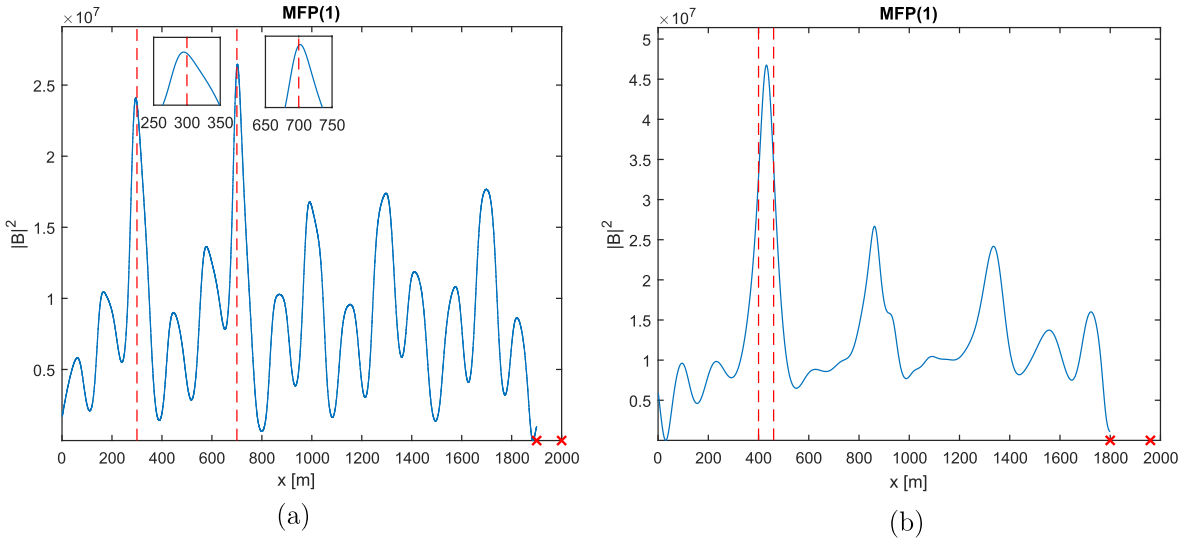

Fig. 2. Double-leak detection using MFP based on the single-leak model. The leak positions are (a) 300 m and 700 m and (b) 400 m and 460 m.

position of contributions from individual leaks. Each individual contribution is a product of the leak size and a function of the corresponding leak location and is independent of other leaks. This property is used later in this paper to formulate an efficient multi-leak detection scheme that identifies leak locations and leak sizes separately.

3.1. Model description

The pipeline system setup is same as in Section 2. A pressure sensor is assumed to be set near the downstream node whose coordinate is denoted by x^M. A model with N leaks is considered, the coordinates of the leaks are $x^{L_n}, n = 1, \ldots, N$, $(x^{L_1} < \cdots < x^{L_N} < x^M)$, z^{L_n} denotes the elevation of the pipe at each leak, and $Q_0^{L_n}$ and $H_0^{L_n}$ are the steady-state discharge and head at each leak. The leak size is represented by the lumped leak parameter $s^{L_n} = C^d A^{L_n}$, where C^d is the discharge coefficient of the leak and A^{L_n} is the flow area of the leak orifice. The steady-state discharge of a leak is related to the lumped leak parameter by $Q_0^{L_n} = s^{L_n}\sqrt{2g(H_0^{L_n} - z^{L_n})}$, in which g is the gravitational acceleration.

The oscillations of discharge (volume rate of water flow) and pressure head due to a fluid transient are represented by q and h. Given the discharge $q(x^U)$ and head $h(x^U)$ at the upstream node x^U, the quantities at x^M can be computed in the following way [35]:

$$\begin{pmatrix} q(x^M) \\ h(x^M) \end{pmatrix} = M^{NL}(x^M - x^{L_N}) \prod_{n=N}^{1} \left\{ \begin{pmatrix} 1 & -\frac{Q_0^{L_n}}{2(H_0^{L_n} - z^{L_n})} \\ 0 & 1 \end{pmatrix} M^{NL}(x^{L_n} - x^{L_{n-1}}) \right\} \begin{pmatrix} q(x^U) \\ h(x^U) \end{pmatrix}, \tag{1}$$

in which $x^{L_0} = x^U$,

$$M^{NL}(x) = \begin{pmatrix} \cosh(\mu x) & -\frac{1}{Z}\sinh(\mu x) \\ -Z\sinh(\mu x) & \cosh(\mu x) \end{pmatrix} \tag{2}$$

is the field matrix, $Z = \mu a^2/(\mathrm{i}\omega g A)$ is the characteristic impedance, $\mu = a^{-1}\sqrt{-\omega^2 + \mathrm{i}gA\omega R}$ is the propagation function, a is the wave speed, ω is the angular frequency, A is the area of pipeline, and R is the frictional resistance term. Note that $R = (FQ_0)/(gDA^2)$ for turbulent flows, in which D is the pipe diameter and Q_0 is the steady-state discharge. If the pipe is frictionless ($F = 0$), $\mu = \mathrm{i}k$ where $k = \omega/a$ is the wavenumber.

In the case of small leaks, i.e., $s^{L_n} \ll 1$, the right hand side of Eq. (1) can be approximated by a linear form being equal to the sum of a term independent of leaks and contributions from various leaks:

$$\begin{pmatrix} q(x^M) \\ h(x^M) \end{pmatrix} \approx \left(M^{NL}(x^M) + \sum_{n=1}^{N} s^{L_n} M^{SL}(L_n, x^{L_n}, x^M) \right) \begin{pmatrix} q(x^U) \\ h(x^U) \end{pmatrix}, \tag{3}$$

in which

$$M^{SL}(L_n, x^{L_n}, x^M) = \sqrt{\frac{g}{2(H_0^{L_n} - z^{L_n})}} \begin{pmatrix} Z\sinh(\mu x^{L_n})\cosh(\mu(x^M - x^{L_n})) & -\cosh(\mu x^{L_n})\cosh(\mu(x^M - x^{L_n})) \\ -Z^2\sinh(\mu x^{L_n})\sinh(\mu(x^M - x^{L_n})) & Z\cosh(\mu x^{L_n})\sinh(\mu(x^M - x^{L_n})) \end{pmatrix} \tag{4}$$

is a matrix related to the location x^{L_n} of the n-th leak (z^{L_n} and $H_0^{L_n}$ are decided by x^{L_n}), but is independent of the other leaks and the size s^{L_n} of n-th leak.

In the following two subsections, the approximation in Eq. (3) is mathematically and numerically verified.

3.2. Mathematical justification of Eq. (3)

The aim of this section is to justify the use of Eq. (3), which will be shown in Theorem 1. To prove this theorem, two lemmas are first given.

Lemma 1. *The matrices M^{NL} and M^{SL} have the following properties:*

(1) $M^{NL}(x_1)M^{NL}(x_2) = M^{NL}(x_1 + x_2)$;
(2) $M^{SL}(L_n, x_1, x_2)M^{NL}(x_3) = M^{SL}(L_n, x_1 + x_3, x_2 + x_3)$;
(3) $M^{NL}(x_1)M^{SL}(L_n, x_2, x_3) = M^{SL}(L_n, x_2, x_1 + x_3)$.

Proof. (1) can be easily obtained from the basic sum rule of hyperbolic functions.

(2):

$$\begin{aligned} &M^{SL}(L_n, x_1, x_2)M^{NL}(x_3) \\ &= \sqrt{\frac{g}{2(H_0^{L_n} - z^{L_n})}} \begin{pmatrix} Z\sinh(\mu x_1)\cosh(\mu(x_2 - x_1)) & -\cosh(\mu x_1)\cosh(\mu(x_2 - x_1)) \\ -Z^2\sinh(\mu x_1)\sinh(\mu(x_2 - x_1)) & Z\cosh(\mu x_1)\sinh(\mu(x_2 - x_1)) \end{pmatrix} \begin{pmatrix} \cosh(\mu x_3) & -\frac{1}{Z}\sinh(\mu x_3) \\ -Z\sinh(\mu x_3) & \cosh(\mu x_3) \end{pmatrix} \\ &= \sqrt{\frac{g}{2(H_0^{L_n} - z^{L_n})}} \begin{pmatrix} Z\sinh(\mu(x_1 + x_3))\cosh(\mu(x_2 - x_1)) & -\cosh(\mu(x_1 + x_3))\cosh(\mu(x_2 - x_1)) \\ -Z^2\sinh(\mu(x_1 + x_3))\sinh(\mu(x_2 - x_1)) & Z\cosh(\mu(x_1 + x_3))\sinh(\mu(x_2 - x_1)) \end{pmatrix} \\ &= M^{SL}(L_n, x_1 + x_3, x_2 + x_3). \end{aligned} \tag{5}$$

(3):

$$\begin{aligned} &M^{NL}(x_1)M^{SL}(L_n, x_2, x_3) \\ &= \sqrt{\frac{g}{2(H_0^{L_n} - z^{L_n})}} \begin{pmatrix} \cosh(\mu x_1) & -\frac{1}{Z}\sinh(\mu x_1) \\ -Z\sinh(\mu x_1) & \cosh(\mu x_1) \end{pmatrix} \begin{pmatrix} Z\sinh(\mu x_2)\cosh(\mu(x_3 - x_2))) & -\cosh(\mu x_2)\cosh(\mu(x_3 - x_2)) \\ -Z^2\sinh(\mu x_2)\sinh(\mu(x_3 - x_2)) & Z\cosh(\mu x_2)\sinh(\mu(x_3 - x_2)) \end{pmatrix} \\ &= \sqrt{\frac{g}{2(H_0^{L_n} - z^{L_n})}} \begin{pmatrix} Z\sinh(\mu x_2)\cosh(\mu(x_1 + x_3 - x_2))) & -\cosh(\mu x_2)\cosh(\mu(x_1 + x_3 - x_2)) \\ -Z^2\sinh(\mu x_2)\sinh(\mu(x_1 + x_3 - x_2)) & Z\cosh(\mu x_2)\sinh(\mu(x_1 + x_3 - x_2)) \end{pmatrix} \\ &= M^{SL}(L_n, x_2, x_1 + x_3). \quad \square \end{aligned} \tag{6}$$

Lemma 2. *Assume that the pipe has N leaks with locations x^{L_n} and sizes s^{L_n} $(n = 1, \ldots, N)$, then the head and discharge at $x^{L_N+}(= \lim_{\delta \to 0+}(x^{L_N} + \delta))$ are*

$$\begin{pmatrix} q(x^{L_N+}) \\ h(x^{L_N+}) \end{pmatrix} = \left(M^{NL}(x^{L_N}) + \sum_{n=1}^{N} s^{L_n} M^{SL}(L_n, x^{L_n}, x^{L_N}) \right) \begin{pmatrix} q(x^U) \\ h(x^U) \end{pmatrix} + o\left(\max_{n=1,\ldots,N}(s^{L_n}) \right) \tag{7}$$

as $\max_{n=1,\ldots,N}(s^{L_n}) \to 0$, where $o(\epsilon)$ stands for an infinitesimal amount with respect to ϵ, i.e., $o(\epsilon)/\epsilon \to 0$.

Proof. In the case of single leak,

$$\begin{pmatrix} q(x^{L_1+}) \\ h(x^{L_1+}) \end{pmatrix} = \begin{pmatrix} 1 & -\frac{Q_0^{L_1}}{2(H_0^{L_1} - z^{L_1})} \\ 0 & 1 \end{pmatrix} M^{NL}(x^{L_1}) \begin{pmatrix} q(x^U) \\ h(x^U) \end{pmatrix} = \left(M^{NL}(x^{L_1}) + s^{L_1} M^{SL}(L_1, x^{L_1}, x^{L_1}) \right) \begin{pmatrix} q(x^U) \\ h(x^U) \end{pmatrix}. \tag{8}$$

Assume that Eq. (7) holds for $N-1$ leaks, then in the case of N leaks,

$$\begin{aligned}
\begin{pmatrix} q(x^{L_N+}) \\ h(x^{L_N+}) \end{pmatrix} &= \begin{pmatrix} 1 & -\frac{Q_0^{L_N}}{2(H_0^{L_N}-z^{L_N})} \\ 0 & 1 \end{pmatrix} M^{NL}(x^{L_N}-x^{L_{N-1}}) \begin{pmatrix} q(x^{L_{N-1}+}) \\ h(x^{L_{N-1}+}) \end{pmatrix} = \left(M^{NL}(x^{L_N}-x^{L_{N-1}}) + s^{L_N} M^{SL}(L_N, x^{L_N}-x^{L_{N-1}}, x^{L_N}-x^{L_{N-1}}) \right) \\
&\quad \left(M^{NL}(x^{L_{N-1}}) + \sum_{n=1}^{N-1} s^{L_n} M^{SL}(L_n, x^{L_n}, x^{L_{N-1}}) + o\left(\max_{n=1,\ldots,N-1}(s^{L_n}) \right) \right) \begin{pmatrix} q(x^U) \\ h(x^U) \end{pmatrix} \\
&= \left(M^{NL}(x^{L_N}) + s^{L_N} M^{SL}(L_N, x^{L_N}, x^{L_N}) + \sum_{n=1}^{N-1} s^{L_n} M^{SL}(L_n, x^{L_n}, x^{L_N}) \right. \\
&\quad \left. + \sum_{n=1}^{N-1} s^{L_n} s^{L_N} M^{SL}(L_N, x^{L_N}-x^{L_{N-1}}, x^{L_N}-x^{L_{N-1}}) M^{SL}(L_n, x^{L_{N-1}}, x^{L_n}) + o\left(\max_{n=1,\ldots,N-1}(s^{L_n}) \right) \right) \begin{pmatrix} q(x^U) \\ h(x^U) \end{pmatrix} \\
&= \left(M^{NL}(x^{L_N}) + \sum_{n=1}^{N} s^{L_n} M^{SL}(L_n, x^{L_n}, x^{L_N}) \right) \begin{pmatrix} q(x^U) \\ h(x^U) \end{pmatrix} + o\left(\max_{n=1,\ldots,N}(s^{L_n}) \right). \quad \square
\end{aligned} \tag{9}$$

Theorem 1. *Assume that the pipe has N leaks with locations x^{L_n} and sizes $s^{L_n}, n = 1, \ldots, N$, then the head and discharge at x^M ($x^M > x^{L_N} > \cdots > x^{L_1}$) is*

$$\begin{pmatrix} q(x^M) \\ h(x^M) \end{pmatrix} = \left(M^{NL}(x^M) + \sum_{n=1}^{N} s^{L_n} M^{SL}(L_n, x^{L_n}, x^M) \right) \begin{pmatrix} q(x^U) \\ h(x^U) \end{pmatrix} + o\left(\max_{n=1,\ldots,N}(s^{L_n}) \right) \tag{10}$$

as $\max_{n=1,\ldots,N}(s^{L_n}) \to 0$.

Proof. The head and discharge at x^M is

$$\begin{pmatrix} q(x^M) \\ h(x^M) \end{pmatrix} = M^{NL}(x^M - x^{L_N}) \begin{pmatrix} q(x^{L_N+}) \\ h(x^{L_N+}) \end{pmatrix}. \tag{11}$$

By Lemmas 1 and 2, Eq. (10) can be directly obtained. □

3.3. Numerical justification of Eq. (3)

In the following, the precision of the approximation given by Eq. (3) is investigated via numerical examples. A single pipe is considered; its characteristic is same as in Section 2. First, it is assumed that the pipe has three leaks at $x^{L_1} = 400$ m, $x^{L_2} = 520$ m and $x^{L_3} = 800$ m. The three leaks have the same size. Two cases of leak sizes $C^d A^L = 8 \times 10^{-4}$ m^2 and $C^d A^L = 3 \times 10^{-4}$ m^2 are considered; correspondingly, the ratio between the leak size and the pipe area is respectively $C^d A^L/A = 4 \times 10^{-3}$ and $C^d A^L/A = 1.5 \times 10^{-3}$. The frequency response function (FRF) at $x^M = 1900$ m due to transient wave from the downstream valve is shown in Fig. 3(a). The solid line and the dash line are obtained from the transfer matrix method Eq. (1) and its linear approximation Eq. (3) respectively. In the case of large leak where $C^d A^L = 8 \times 10^{-4}$ m^2, the shape of FRF is well-replicated but at resonant frequencies the error is relatively large. For the smaller leak size $C^d A^L = 3 \times 10^{-4}$ m^2, the amplitudes at all frequencies are accurate. Similarly, the results of two cases of double-leak are displayed in Fig. 3(b) $x^{L_1} = 400$ m, $x^{L_2} = 520$ m and (c) $x^{L_1} = 400$ m, $x^{L_2} = 460$ m. In both cases, the FRF for the larger leak size $C^d A^L = 8 \times 10^{-4}$ m^2 is better replicated using the linear approximation Eq. (3).

The average relative error (RE) of FRF with respect to leak size is also studied and plotted in Fig. 4. Here, the average RE is defined by

$$\overline{\mathrm{RE}} = \frac{1}{30\omega_{th}} \int_{\omega_{th}}^{31\omega_{th}} \left| \frac{\|\tilde{h}(x^M, \omega)\| - \|h(x^M, \omega)\|}{\|h(x^M, \omega)\|} \right| d\omega, \tag{12}$$

where h and $\tilde{h}$ are pressure heads obtained from Eqs. (1) and (3), respectively. The three cases of leak locations are considered here again: (i) $x^{L_1} = 400$ m, $x^{L_2} = 520$ m and $x^{L_3} = 800$ m; (ii) $x^{L_1} = 400$ m and $x^{L_2} = 520$ m; (iii) $x^{L_1} = 400$ m and $x^{L_2} = 460$ m. In all three cases the approximation precision decreases as the leak size increases. However, for a small leak size (the main concern in the leakage detection problem), say $C^d A^L \leqslant 2 \times 10^{-4}$ m^2 ($C^d A^L/A = 1 \times 10^{-3}$), the approximation errors for all the three cases are acceptable: the average RE is always less than 2%. Furthermore, Fig. 4 also shows that

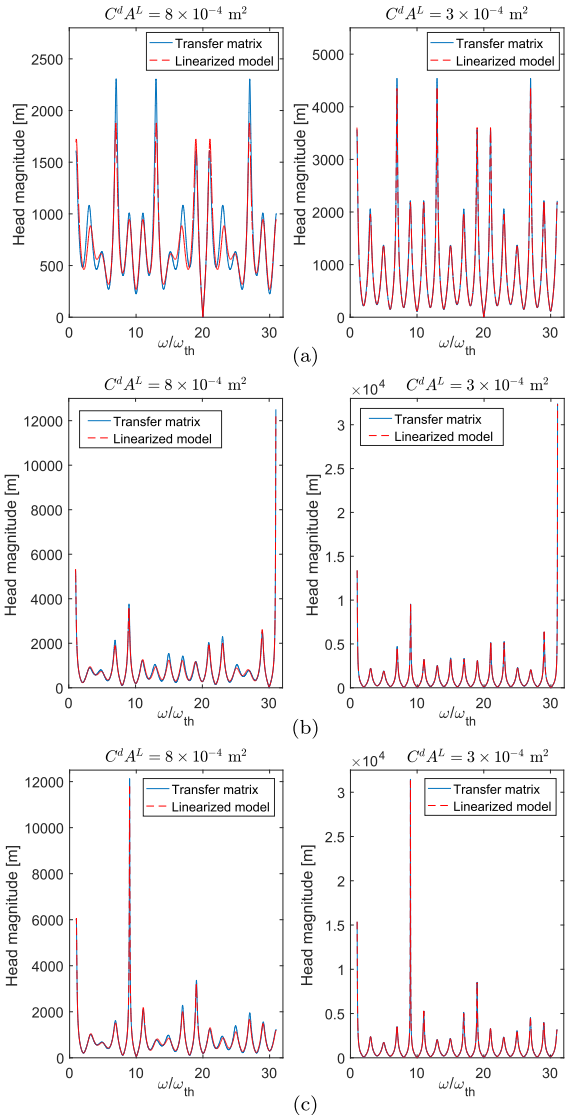

Fig. 3. Frequency response function (head magnitude) at $x^M = 1900$ m obtained from the transfer matrix method (solid line) and the linearized model (dash line). The leak locations are (a) $x^{L_1} = 400$ m, $x^{L_2} = 520$ m and $x^{L_3} = 800$ m; (b) $x^{L_1} = 400$ m and $x^{L_2} = 520$ m; (c) $x^{L_1} = 400$ m and $x^{L_2} = 460$ m. The leak size is $C^dA^L = 8 \times 10^{-4}$ m^2 (left) and $C^dA^L = 3 \times 10^{-4}$ m^2 (right). The pipe length is $l = 2000$ m.

the three-leak case has a larger error than the other two cases. Besides, a larger distance between the two leaks introduces a slight increase of FRF error.

4. Maximum likelihood estimation of multiple leaks

4.1. Data model

In this section, multiple leaks are again estimated by the ML approach but this time in the presence of white noise. The head measurement at the station x_m $(m = 1, \ldots, M)$ near the downstream for the frequency ω_j $(j = 1, \ldots, J)$ is assumed to follow the theoretical expression from Eq. (3) plus a noise term:

$$h(\omega_j, x_m) = h^{NL}(\omega_j, x_m) + \sum_{n=1}^{N} s^{L_n} G(\omega_j, x^{L_n}, x_m) + n_{jm}, \tag{13}$$

wherein

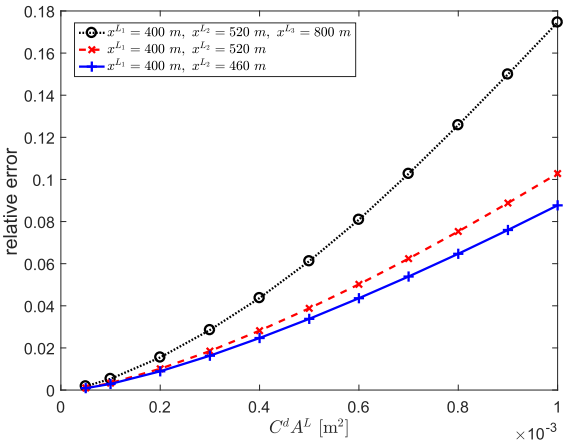

Fig. 4. Average relative error of FRF due to model linearization with respect to leak size C^dA^L. The measurement station locates at $x^M = 1900$ m. The leak locations are (i) $x^{L_1} = 400$ m, $x^{L_2} = 520$ m and $x^{L_3} = 800$ m; (ii) $x^{L_1} = 400$ m and $x^{L_2} = 520$ m; (iii) $x^{L_1} = 400$ m and $x^{L_2} = 460$ m. The pipe length is $l = 2000$ m.

$$h^{NL}(\omega_j, x_m) = -Z\sinh(\mu x_m)q(x^U) + \cosh(\mu x_m)h(x^U), \tag{14}$$

$$G(\omega_j, x^{L_n}, x_m) = -\frac{\sqrt{g}Z\sinh\left(\mu(x_m - x^{L_n})\right)}{\sqrt{2(H_0^{L_n} - z^{L_n})}}\left(Z\sinh\left(\mu x^{L_n}\right)q(x^U) - \cosh\left(\mu x^{L_n}\right)h(x^U)\right), \tag{15}$$

and n_{jm}'s are independent random variables and follow Gaussian random distribution with 0-mean and variance σ^2. It is noticeable that the noise is assumed to be white noise, i.e., the power (variance) is constant with various frequencies. For non-white noise, the signal can be whitened such that the white noise assumption is satisfied [34]. Note that the discharge $q(x^U)$ at the upstream node x^U can be estimated by adding a measurement station near the upstream boundary [36,37], denoted by $x^U + \epsilon$, and assuming there is no leak between x^U and $x^U + \epsilon$. Using the pressure head measurement $h(x^U + \epsilon)$ at $x^U + \epsilon$ and applying a boundary condition $h(x^U)$ of head at x^U, the discharge at the upstream node $q(x^U)$ can be solved via

$$\begin{pmatrix} q(x^U) \\ h(x^U) \end{pmatrix} = M^{NL}(-\epsilon)\begin{pmatrix} q(x^U + \epsilon) \\ h(x^U + \epsilon) \end{pmatrix} = \begin{pmatrix} \cosh(\mu\epsilon) & \frac{1}{Z}\sinh(\mu\epsilon) \\ Z\sinh(\mu\epsilon) & \cosh(\mu\epsilon) \end{pmatrix}\begin{pmatrix} q(x^U + \epsilon) \\ h(x^U + \epsilon) \end{pmatrix}, \tag{16}$$

that is,

$$\hat{q}(x^U) = \frac{\cosh(\mu\epsilon)h(x^U) - h(x^U + \epsilon)}{Z\sinh(\mu\epsilon)}. \tag{17}$$

Let $\Delta h_{jm} \equiv h(\omega_j, x_m) - h^{NL}(\omega_j, x_m)$ denote the head difference between the head measurement in the presence of leaks and the theoretical head that does not include the leak terms at the frequency ω_j and at the measurement station x_m, and denote

$$\Delta\mathbf{h} = (\Delta h_{11}, \ldots, \Delta h_{J1}, \ldots, \Delta h_{1M}, \ldots, \Delta h_{JM})^\top, \tag{18}$$

then we have the following equation:

$$\Delta\mathbf{h} = \mathbf{G}(\mathbf{x}^L)\mathbf{s}^L + \mathbf{n}. \tag{19}$$

In this equation, $\mathbf{G}$ is a $JM \times N$-dimensional matrix whose n-th column is

$$\mathbf{G}_n(x^{L_n}) = (G(\omega_1, x^{L_n}, x_1), \ldots, G(\omega_J, x^{L_n}, x_1), \ldots, G(\omega_1, x^{L_n}, x_M), \ldots, G(\omega_J, x^{L_n}, x_M))^\top, \tag{20}$$

$$\mathbf{x}^L = (x^{L_1}, \ldots, x^{L_N})^\top, \quad \mathbf{s}^L = (s^{L_1}, \ldots, s^{L_N})^\top, \tag{21}$$

and

$$\mathbf{n} = (n_{11}, \ldots, n_{J1}, \ldots, n_{1M}, \ldots, n_{JM})^\top. \tag{22}$$

In the following, the data $\Delta\mathbf{h}$ will be used to estimate the leak locations $\mathbf{x}^L$ and sizes $\mathbf{s}^L$.

4.2. Maximum likelihood estimation for leak locations and sizes

Since the vector of head difference $\Delta\mathbf{h}$ follows a JM-dimensional complex-valued Gaussian distribution, its probability density function (PDF) is

$$p(\Delta\mathbf{h};\mathbf{x}^L,\mathbf{s}^L)=(\pi\sigma^2)^{-JM}\exp\left(-\frac{1}{\sigma^2}\left\|\Delta\mathbf{h}-\mathbf{G}(\mathbf{x}^L)\mathbf{s}^L\right\|^2\right). \tag{23}$$

Therefore, the log-likelihood function is

$$\log L(\mathbf{x}^L,\mathbf{s}^L;\Delta\mathbf{h})=-JM\log(\pi\sigma^2)-\frac{1}{\sigma^2}\|\Delta\mathbf{h}-\mathbf{G}(\mathbf{x}^L)\mathbf{s}^L\|^2. \tag{24}$$

The ML estimation of the parameters $\mathbf{x}^L$ and sizes $\mathbf{s}^L$ are obtained by maximizing Eq. (24):

$$\{\hat{\mathbf{x}}^L,\hat{\mathbf{s}}^L\}=\arg\max_{\mathbf{x}^L,\mathbf{s}^L}\log L(\Delta\mathbf{h};\mathbf{x}^L,\mathbf{s}^L)=\arg\min_{\mathbf{x}^L,\mathbf{s}^L}\|\Delta\mathbf{h}-\mathbf{G}(\mathbf{x}^L)\mathbf{s}^L\|^2. \tag{25}$$

For any $\mathbf{x}^L$, the corresponding estimate of $\mathbf{s}^L$ has the form of least square (LS) solution:

$$\mathbf{s}^L=\left(\mathbf{G}^H(\mathbf{x}^L)\mathbf{G}(\mathbf{x}^L)\right)^{-1}\mathbf{G}^H(\mathbf{x}^L)\Delta\mathbf{h}. \tag{26}$$

Therefore, by inserting Eq. (26) into Eq. (25), the estimate of N leak locations are obtained:

$$\hat{\mathbf{x}}^L=\arg\min_{\mathbf{x}^L}\left\|\Delta\mathbf{h}-\mathbf{G}(\mathbf{x}^L)\left(\mathbf{G}^H(\mathbf{x}^L)\mathbf{G}(\mathbf{x}^L)\right)^{-1}\mathbf{G}^H(\mathbf{x}^L)\Delta\mathbf{h}\right\|^2=\arg\max_{\mathbf{x}^L}\left(\Delta\mathbf{h}^H\mathbf{G}(\mathbf{x}^L)\left(\mathbf{G}^H(\mathbf{x}^L)\mathbf{G}(\mathbf{x}^L)\right)^{-1}\mathbf{G}^H(\mathbf{x}^L)\Delta\mathbf{h}\right). \tag{27}$$

The size estimates of the N leaks are then obtained by

$$\hat{\mathbf{s}}^L=\left(\mathbf{G}^H(\hat{\mathbf{x}}^L)\mathbf{G}(\hat{\mathbf{x}}^L)\right)^{-1}\mathbf{G}^H(\hat{\mathbf{x}}^L)\Delta\mathbf{h}. \tag{28}$$

Finally, the multiple-leak identification algorithm using the ML approach is summarized in Algorithm 1.

Algorithm 1. Maximum likelihood approach for multiple-leak detection

1. Select J frequencies $\omega_1,\ldots,\omega_J$;
2. Estimate the discharge at the upstream $q(x^U)$ from Eq. (17);
3. Calculate h_{jm}^{NL} at the j-th frequencies and m-th measurement station ($j=1,\ldots,J, m=1,\ldots,M$) via Eq. (14) and use the head differences Δh_{jm} as the data;
4. Estimate the locations of the N leaks by solving the maximization problem Eq. (27);
5. Estimate the size of the N leaks from Eq. (28).

5. Analytical properties of the maximum likelihood leak detection

The analytical properties of the proposed ML method are introduced in this section. The equivalence to matched-field and matched-filter approaches is also presented.

5.1. Properties of maximum likelihood and Cramér-Rao lower bound

The proposed leak identification method inherits the properties of maximum likelihood estimation (MLE). More specifically, the estimates converge in probability to the actual leak positions and sizes and the variance of each estimator achieves the CRLB when the sample size tends to infinity [38]. The latter implies that the proposed estimator has the lowest mean squared error (MSE) for large sample size. A brief introduction of CRLB can be found in Appendix A. The CRLBs of leak locations and sizes, denoted as $\Theta=\{\mathbf{x}^L,\mathbf{s}^L\}$, are given by

$$\mathrm{Cov}(\hat{\Theta})\geqslant CRLB(\Theta)=(T\mathbf{I}(\Theta))^{-1}, \tag{29}$$

in which T is the sample size and $\mathbf{I}(\Theta)$ is the Fisher information matrix (FIM):

$$\mathbf{I}(\Theta)=\frac{1}{\sigma^2}\begin{pmatrix}diag(\mathbf{s}^L) & \mathbf{0}\\ \mathbf{0} & \mathbf{I}_N\end{pmatrix}\begin{pmatrix}(\mathbf{G}')^H\mathbf{G}'+\left((\mathbf{G}')^H\mathbf{G}'\right)^\top & (\mathbf{G}')^H\mathbf{G}+\left(\mathbf{G}^H\mathbf{G}'\right)^\top\\ \mathbf{G}^H\mathbf{G}'+\left((\mathbf{G}')^H\mathbf{G}\right)^\top & \mathbf{G}^H\mathbf{G}+\left(\mathbf{G}^H\mathbf{G}\right)^\top\end{pmatrix}\begin{pmatrix}diag(\mathbf{s}^L) & \mathbf{0}\\ \mathbf{0} & \mathbf{I}_N\end{pmatrix}. \tag{30}$$

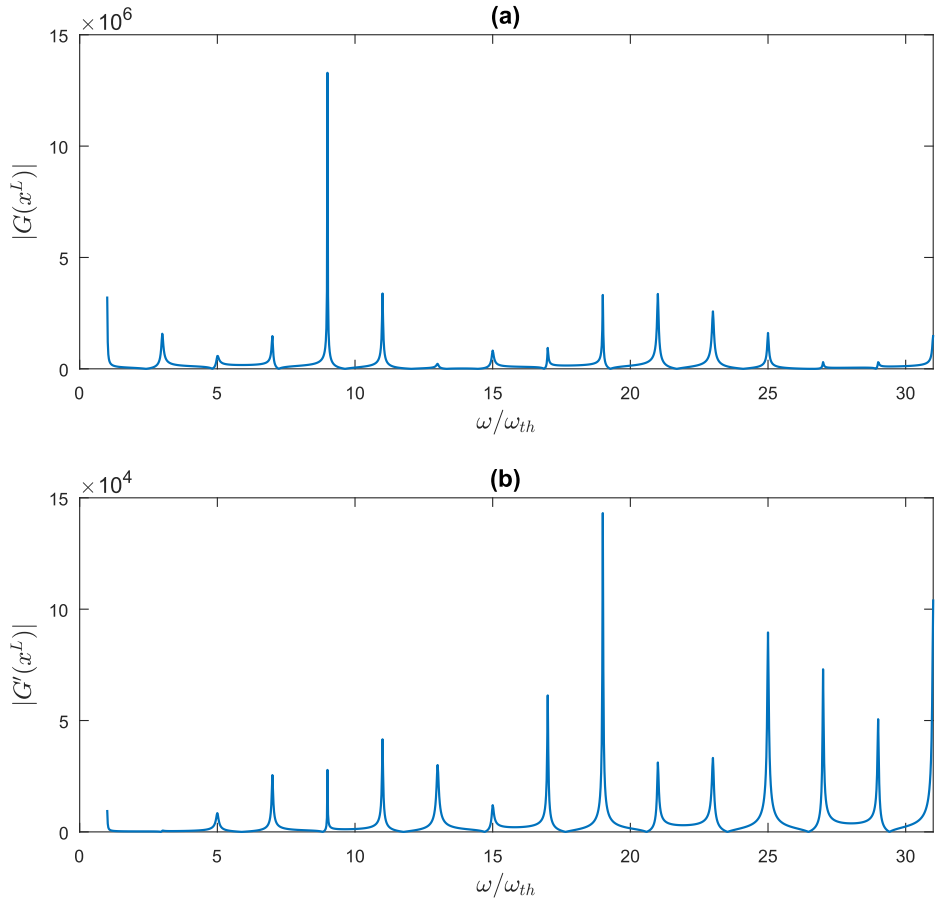

Fig. 5. $|G|$ and $|G'|$ as a function of normalized frequencies ω/ω_{th} at $x^M = 1980$ m. The pipe has a single leak at $x^L = 300$ m and the pipe length is $l = 2000$ m.

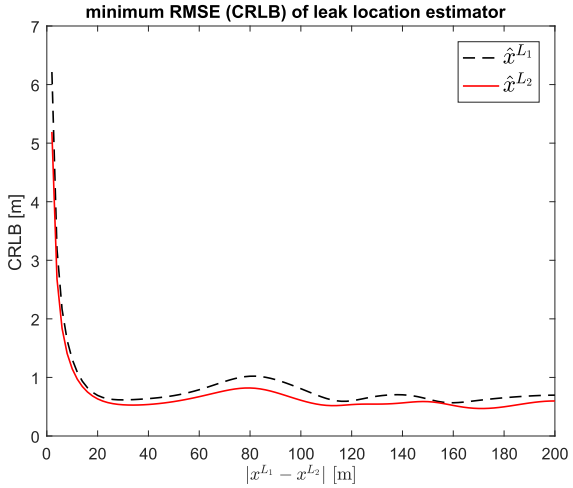

Fig. 6. CRLB of RMSE of the estimator $\hat{x}^{L_1}$ and $\hat{x}^{L_2}$ with respect to leak distance. The leak locations are $x^{L_1} = 400$ m and $x^{L_2} \in [402, 600]$. The minimum wavelength is 258 m.

The CRLBs of $\hat{x}^{L_n}$ and $\hat{s}^{L_n}$, which represent the minimum achievable MSE, are n-th and $(N+n)$-th diagonal elements of $CRLB(\Theta)$. The detailed derivation can be found in Appendix B.

Fig. 5 shows an example that plots $|G(\omega, x^L, x^M)|$ and $\left|\frac{\partial G(\omega, x^L, x^M)}{\partial x^L}\right|$ as a function of normalized angular frequency ω/ω_{th} at $x^M = 1980$ m and the leak location is $x^L = 300$ m (the pipe length is $l = 2000$ m). Both plots have higher amplitude at resonant frequencies, implying that these frequencies bring more information and contribute more to leak detection precision than others, according to Eqs. (29) and (30). However, using more frequencies, as well as more sensors, pushes down the CRLB for both leak location and size estimators and is thus preferable.

In Fig. 6, another example is considered, wherein two leaks exist in a pipe. Fig. 6 plots the CRLBs for estimators of both leak locations $\hat{x}^{L_1}$ and $\hat{x}^{L_2}$ with respect to various leak distances. More exactly, the leak locations are $x^{L_1} = 400$ m and $x^{L_2} \in [402, 600]$. The minimum wavelength of probing wave is 258 m. Note that when the two leaks are close to each other meaning that $|\hat{x}^{L_1} - \hat{x}^{L_2}| < \lambda_{min}/2$ (but greater than around 20 m), the CRLB stays at almost the same level (approximately 1 m), which implies that detecting reliably two very close leaks is inherent in the proposed ML method according to the convergence property of ML. When the distance between the two leaks tends to zero, the CRLB dramatically increases, which implies that two very close leaks cannot be localized accurately no matter which detection method is used. The reason is that in this case the measurement does not bring enough information (e.g., too narrow bandwidth of probing wave) for the desired parameter estimation. Note that the result in Fig. 6 is obtained with sample size $T = 1$. When more data are available, the CRLB, as well as the minimum resolvable distance between leaks, can be further decreased, which can be justified by Eq. (29). More detailed discussion and numerical analysis concerning the resolution (the capacity to separately estimate two close leaks) of leak characterization methods is presented in Section 6.

5.2. Equivalence to matched-field and matched-filter approaches

In the following, the proposed ML method is proved to be equivalent to the MFP and the matched-filter method [39–42] under the multi-leak model. This means that the proposed ML method equally maximizes the SNR and is thus robust with respect to noise. Note that the MFP and the matched-filter method mentioned in this section are different with the ones in Ref. [34] where a single leak is assumed in the model. More specifically, two parameters (location and size of the single leak) are estimated in Ref. [34], while $2N$ parameters are considered in the present paper.

MFP uses a weighting vector $\mathbf{w}$ with unit norm ($\|\mathbf{w}\| = 1$) to match the measurement $\Delta\mathbf{h}$ by maximizing

$$|B|^2 = |\mathbf{w}^H \Delta\mathbf{h}|^2 = \mathbf{w}^H \Delta\mathbf{h}\Delta\mathbf{h}^H \mathbf{w}. \tag{31}$$

By replacing $\Delta\mathbf{h}$ by Eq. (19) and maximizing the expectation of Eq. (31), the optimal weight $\mathbf{w}$ is obtained by

$$\hat{\mathbf{w}} = \arg\max_{\mathbf{w}} \mathbb{E}(|B|^2) = \arg\max_{\mathbf{w}} \left(\mathbf{w}^H \mathbf{G}\mathbf{s}^L (\mathbf{s}^L)^H \mathbf{G}^H \mathbf{w} + \sigma^2\right) = \arg\max_{\mathbf{w}} \left|\mathbf{w}^H \left(\mathbf{G}\mathbf{s}^L\right)\right|^2 = \frac{\mathbf{G}\mathbf{s}^L}{\left\|\mathbf{G}\mathbf{s}^L\right\|}. \tag{32}$$

The last equality holds due to the property of inner product. By inserting Eq. (32) into Eq. (31), the model parameters can be estimated:

$$\{\hat{\mathbf{x}}^L, \hat{\mathbf{s}}^L\} = \arg\max_{\mathbf{x}^L, \mathbf{s}^L} \frac{\left|\Delta\mathbf{h}^H \mathbf{G}(\mathbf{x}^L)\mathbf{s}^L\right|^2}{\|\mathbf{G}(\mathbf{x}^L)\mathbf{s}^L\|^2}. \tag{33}$$

Note that for any fixed $\mathbf{x}^L$, the right hand side of Eq. (33) can be seen as maximizing a ratio of two quadratic forms of $\mathbf{s}^L$, also known as the generalized Rayleigh quotient, which has the solution

$$\hat{\mathbf{s}}^L = \left(\mathbf{G}^H(\mathbf{x}^L)\mathbf{G}(\mathbf{x}^L)\right)^{-1} \mathbf{G}^H(\mathbf{x}^L)\Delta\mathbf{h}. \tag{34}$$

The derivation of Eq. (34) can be found in Appendix C. Inserting Eq. (34) into Eq. (33) results in the estimate of $\mathbf{x}^L$:

$$\hat{\mathbf{x}}^L = \arg\max_{\mathbf{x}^L} \frac{\left|\Delta\mathbf{h}^H \mathbf{G}(\mathbf{x}^L)\left(\mathbf{G}^H(\mathbf{x}^L)\mathbf{G}(\mathbf{x}^L)\right)^{-1} \mathbf{G}^H(\mathbf{x}^L)\Delta\mathbf{h}\right|^2}{\left\|\mathbf{G}(\mathbf{x}^L)\left(\mathbf{G}^H(\mathbf{x}^L)\mathbf{G}(\mathbf{x}^L)\right)^{-1} \mathbf{G}^H(\mathbf{x}^L)\Delta\mathbf{h}\right\|^2} = \arg\max_{\mathbf{x}^L} \Delta\mathbf{h}^H \mathbf{G}(\mathbf{x}^L)\left(\mathbf{G}^H(\mathbf{x}^L)\mathbf{G}(\mathbf{x}^L)\right)^{-1} \mathbf{G}^H(\mathbf{x}^L)\Delta\mathbf{h}. \tag{35}$$

Therefore, the equivalence between the MLE and the MFP is proved.

The matched-filter approach applies a filter $\mathbf{w}$ to the head difference

$$\mathbf{w}^H \Delta\mathbf{h} = \mathbf{w}^H \mathbf{G}\mathbf{s}^L + \mathbf{w}^H \mathbf{n}, \tag{36}$$

such that the SNR reaches its maximum, i.e., to find the optimal filter

$$\hat{\mathbf{w}} = \arg\max_{\mathbf{w}} \frac{\left|\mathbf{w}^H \mathbf{G}\mathbf{s}^L\right|^2}{\mathbb{E}\left(|\mathbf{w}^H \mathbf{n}|^2\right)} = \arg\max_{\mathbf{w}} \frac{\left|\mathbf{w}^H \mathbf{G}\mathbf{s}^L\right|^2}{\sigma^2 \|\mathbf{w}\|^2} = \arg\max_{\mathbf{w}} \left|\frac{\mathbf{w}^H}{\|\mathbf{w}\|} \mathbf{G}\mathbf{s}^L\right|^2. \tag{37}$$

To obtain a non-trivial solution, the filter is assumed to have a unit norm, i.e., $\|\mathbf{w}\| = 1$, thus

$$\hat{\mathbf{w}} = \frac{\mathbf{G}\mathbf{s}^L}{\left\|\mathbf{G}\mathbf{s}^L\right\|}, \tag{38}$$

which is identical to the optimal weight of MFP (Eq. (32)). The above presentation illustrates that the proposed ML approach minimizes the influence of noise and is thus robust in a noisy environment.

6. Numerical simulations

In this section, numerical examples are introduced, where the performance of the ML method based on the model of multiple leaks is compared with the MFP method based on the single leak model introduced in Ref. [34]. Note that the MFP is equivalent to the ML method with single-leak assumption. To avoid confusion in this section, MLE refers to the ML method based on the model of multiple leaks and MFP(1) refers to the ML method with single-leak model. The numerical simulation test system is shown in Fig. 1. The cases introduced in Fig. 2 are considered to illustrate the improvement of multiple-leak detection by the proposed method (i.e., MLE) over the MFP(1). Note that the wave propagation simulation in the forward problem is accomplished using the transfer matrix method while in the inverse problem the linearized model is used.

First, the case in Fig. 2(a) is considered, i.e., two leaks at $x^{L_1} = 300$ m and $x^{L_2} = 700$ m with sizes $s^{L_1} = 1 \times 10^{-4}$ m^2 and $s^{L_2} = 1.2 \times 10^{-4}$ m^2 (the relative leak size $C^d A^{L_1}/A = 0.5 \times 10^{-3}$ and $C^d A^{L_2}/A = 0.6 \times 10^{-3}$). The boundary condition $h(x^U) = 0$ is applied and $q(x^U)$ is calculated from Eq. (17) by measuring the head pressure at $x^{M_0} = 50$ m. The measurements from the other two transducers at $x^{M_1} = 1800$ m and $x^{M_2} = 1960$ m are used in the leak estimation process. Gaussian white noise with $\mathbf{0}$-mean is added to the head measurements from all three transducers (at x^{M_0}, x^{M_1} and x^{M_2}). Here, the SNR is 10 dB, which is defined by

$$\mathrm{SNR} = 20\log_{10}\left(\overline{|\mathbb{E}(\Delta\mathbf{h})|}/\sigma\right) = 20\log_{10}\left(\frac{s^L}{\sigma}\overline{|\mathbf{G}|}\right), \tag{39}$$

where $\overline{|\mathbb{E}(\Delta\mathbf{h})|}$ stands for the average head difference and σ is the standard deviation of the Gaussian white noise. It can be seen from Eq. (39) that increasing SNR is equivalent to increasing the leak size s^L or decreasing the noise standard deviation σ. Furthermore, the influence of the steady-state pressure head $H_0^{L_n}$ at n-th leak, which also affect the localization accuracy [24,43], can be equivalently quantified by varying SNR, since its square root is proportional to the leak size s^{L_n} when $z^{L_n} = 0$ (cf. Eqs. (13) and (15)). Therefore, although this section shows the simulation results with varying SNR and fixed s^{L_n} and $H_0^{L_n}$, their influences are equivalently quantified. The frequencies $\omega = \{(1+\alpha)\omega_{th} : \alpha = 0, 0.02, 0.04, \ldots, 30\}$ are used. In the results obtained from MFP(1), the estimates of both leaks have slight errors (the two local maxima are at 295 m and 703 m in Fig. 2(a)). Fig. 7(a) displays the objective function of MLE (Eq. (27)) under the two-leak assumption, which reaches a maximum corresponding to the estimated locations of the leaks. The estimate is very close to the actual location, which is represented by the cross in the figure. The leak sizes are estimated via Eq. (28), being $\hat{s}^{L_1} = 1.025 \times 10^{-4}$ m^2 (the actual value is 1×10^{-4} m^2) and $\hat{s}^{L_2} = 1.188 \times 10^{-4}$ m^2 (the actual value is 1.2×10^{-4} m^2). Fig. 7(b) shows the comparison between the MLE (circles) and the actual values (lines) in terms of the leak location (x-axis) and size (y-axis). Since the results are affected by random error, particularly for low SNR, each simulation (from data generation to leak estimation) is repeated 30 times. Fig. 8 shows the root mean square error (RMSE) of localization using both methods with respect to various SNR ($-3, 0, 3, 6, 9$ dB), along with CRLB, which here is actually the square root of Eq. (29), i.e., the lower limit of RMSE. Here, RMSE is defined by

$$RMSE(\hat{\mathbf{x}}^L) = \left(\overline{e^2(\hat{\mathbf{x}}^L)}\right)^{\frac{1}{2}}, \tag{40}$$

in which the overline stands for the average and $e(\hat{\mathbf{x}}^L)$ is the L_2-error between the actual and estimated locations of the leaks:

$$e(\hat{\mathbf{x}}^L) = \|\mathbf{x}^L - \hat{\mathbf{x}}^L\|_{L_2} = \sqrt{\left(x^{L_1} - \hat{x}^{L_1}\right)^2 + \left(x^{L_2} - \hat{x}^{L_2}\right)^2}. \tag{41}$$

Note that Eqs. (40) and (41) have the dimension of length, which is deliberate because it helps to define the errors in physical units. It is clear that MFP(1) has a much larger error while MLE is very accurate with a RMSE less than 1 m for all SNRs and very close to the CRLB.[1] The reason is that, as previously stated, the error of MFP(1) comes from not only the noise but also the imprecise (non-parameterized) model. It is remarkable that the RMSE of MLE can converge to the CRLB but it requires a large sample size; here, however, only one experimental result ($T = 1$) is used for leak detection, even so the RMSE is very close to the CRLB.

Next, two close leaks are considered, i.e., the case in Fig. 2(b), whose locations are $x^{L_1} = 400$ m and $x^{L_2} = 460$ m. The frequencies used for leak detection are the same as the previous case, implying that the minimum wavelength is $\lambda_{min} = 258$ m.

[1] Here, CRLB corresponds to the lower bound of Eq. (41) and is thus obtained from $\sqrt{CRLB(x^{L_1}) + CRLB(x^{L_2})}$.

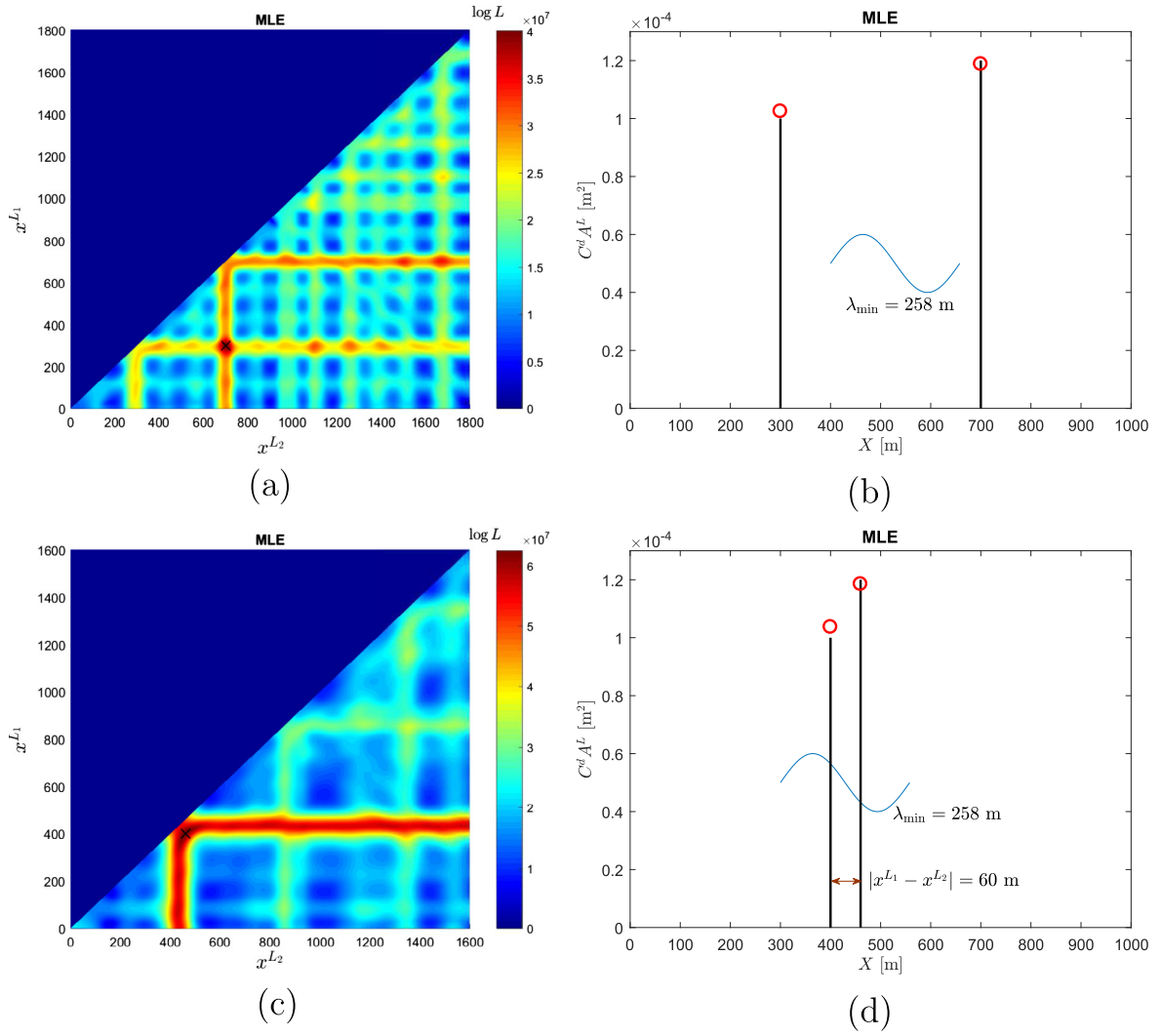

Fig. 7. Double-leak detection using MLE. The leak positions are (a,b) 300 m and 700 m and (c,d) 400 m and 460 m. Subfigures (a) and (c) plot the 2D objective function in Eq. (27). Subfigures (b) and (d) show the locations and sizes of actual (lines) and estimated (circles) leaks.

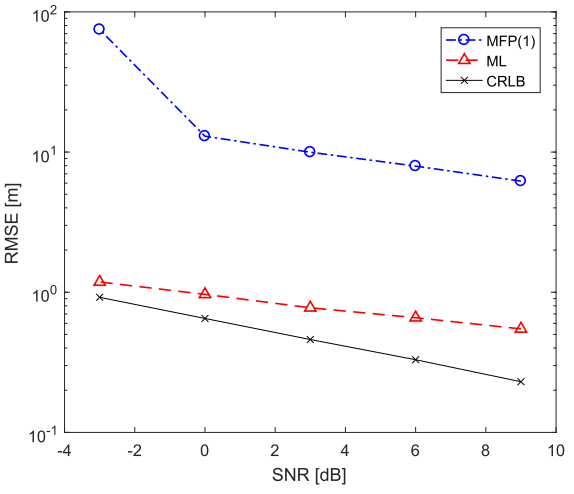

Fig. 8. Leak localization error using MFP(1) and MLE. The leak locations are $x^{L_1} = 300$ m and $x^{L_2} = 700$ m.

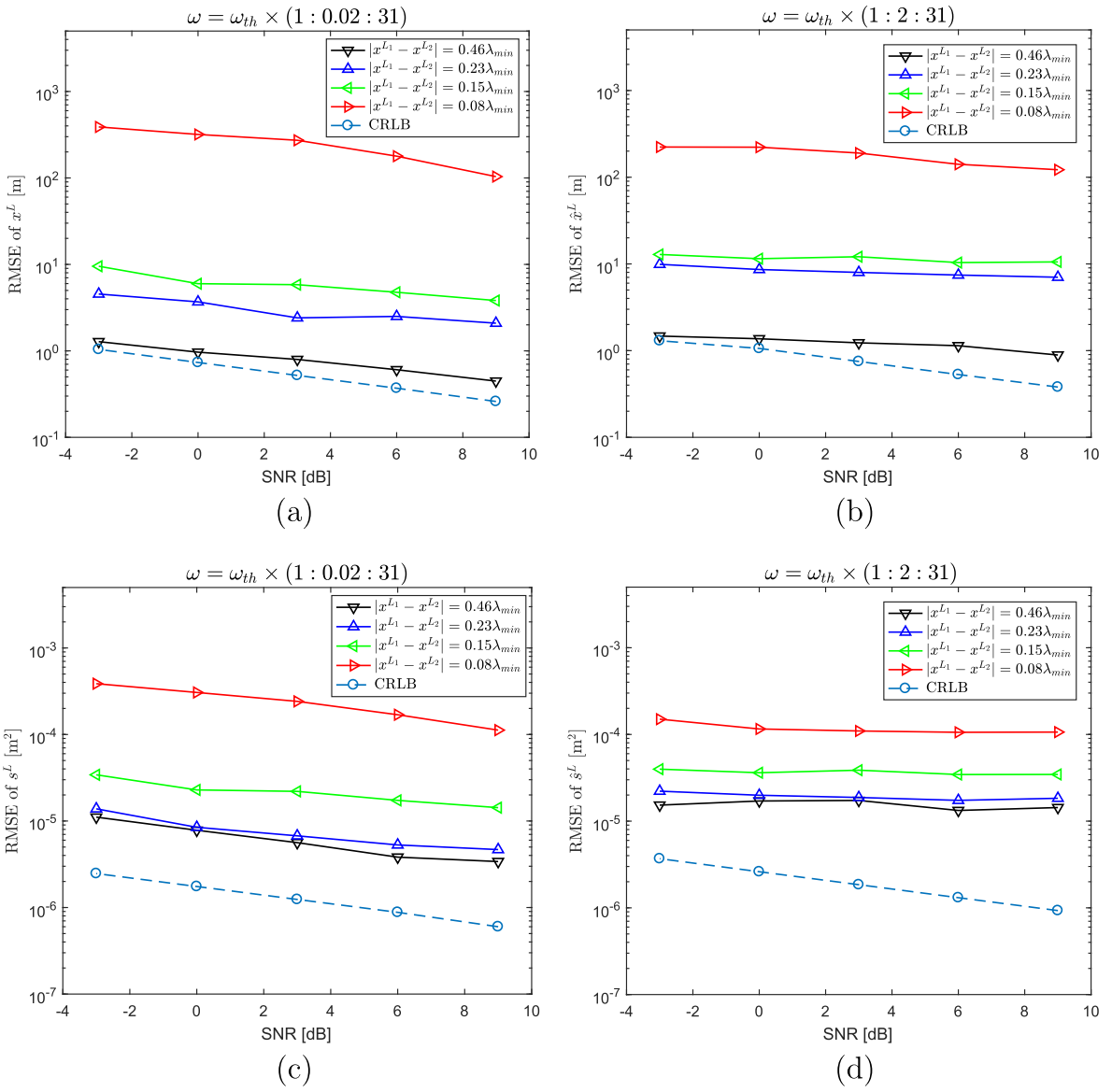

Fig. 9. RMSEs of leak localization (a,b) and size estimation (c,d) with respect to SNR $(-3, 0, 3, 6, 9$ dB). Frequencies used are (a,c) $\omega = \{(1+\alpha)\omega_{th} : \alpha = 0, 0.02, 0.04, \ldots, 30\}$ and (b,d) $\omega = \{(1+\alpha)\omega_{th} : \alpha = 0, 2, 4, \ldots, 30\}$. The distance between the two leaks is $0.46\lambda_{min}, 0.23\lambda_{min}, 0.15\lambda_{min}$, and $0.08\lambda_{min}$.

On the other hand, the leak distance is $|x^{L_1} - x^{L_2}| = 60\text{m} = 0.23\lambda_{min}$. In this case, as indicated in Ref. [34] as well as the Nyquist-Shannon sampling theorem, since the distance between the two leaks is less than the half minimum wavelength, MFP(1) cannot separately identify the two leaks (cf. Fig. 2(b)). However, it is clear that the MLE is not limited by this minimum resolvable range and returns a super-resolution estimate: as is illustrated in Fig. 7(c) and (d), in this case $(|x^{L_1} - x^{L_2}| < \lambda_{min}/4)$ both the locations and sizes of the two leaks are accurately estimated.

Fig. 9(a) shows the leak localization error with respect to various SNR and leak distances $|x^{L_1} - x^{L_2}| = 0.08\lambda_{min}, 0.15\lambda_{min}, 0.23\lambda_{min}, 0.46\lambda_{min}$. Again, the RMSE is shown in the figures and is obtained from 30 simulation results. The CRLB (corresponding to the lower bound of RMSE as in the previous example) for the case $|x^{L_1} - x^{L_2}| = 0.46\lambda_{min}$ is also shown; actually the CRLBs for all the four cases are very close, thus only one of them is shown. For any leak location, the localization error increases as SNR decreases. Also, for a given SNR, decreasing the distance between the two leaks increases the localization error, which implies that a shorter distance results in a more sensitive localization result with respect to error. However, the error for the range $|x^{L_1} - x^{L_2}| \geqslant 0.15\lambda_{min}$ is acceptable: RMSE is less than 10 m even for a very low SNR of -3 dB. A further advantage of the proposed method is that it is not limited to resonant frequencies but can use

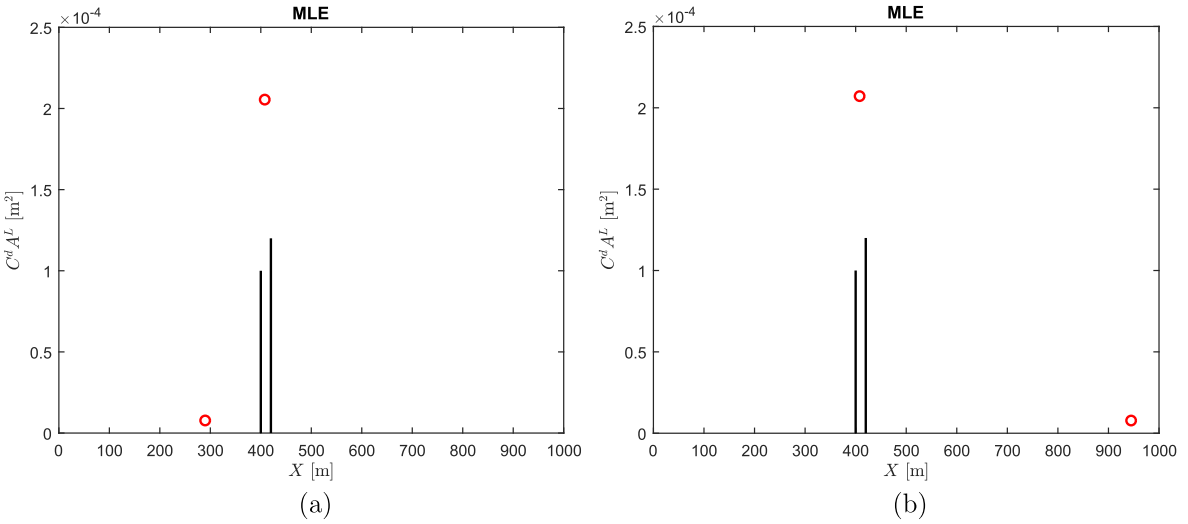

Fig. 10. Two ML identification results of double leaks. The leak locations are $x^{L_1} = 400$ m and $x^{L_2} = 420$ m and the leak sizes are $s^{L_1} = 1 \times 10^{-4}$ m^2 and $s^{L_2} = 1.2 \times 10^{-4}$ m^2. The lines and circles stand for the actual and estimated leaks, respectively.

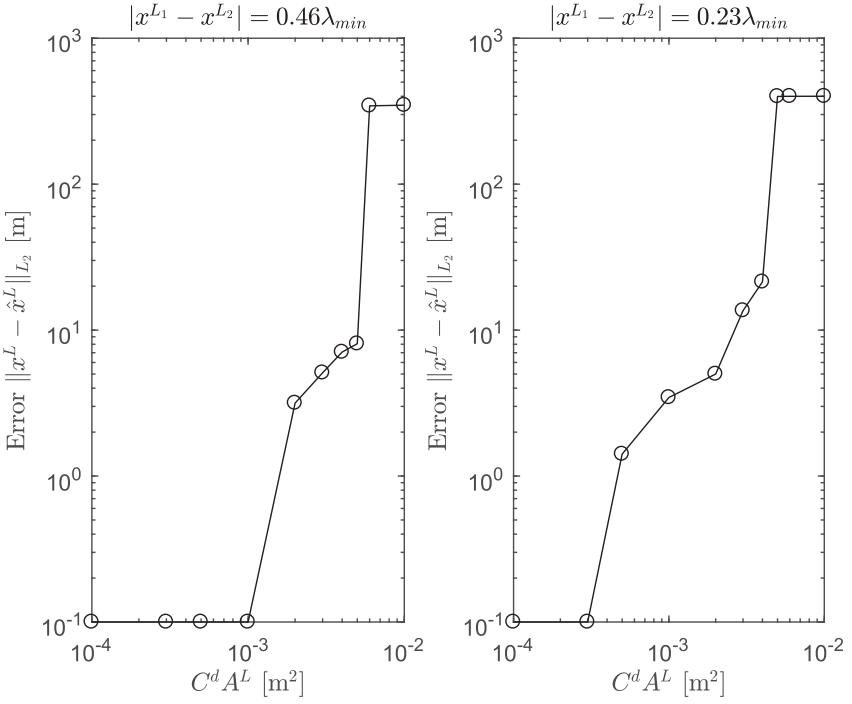

Fig. 11. Leak localization error with respect to leak size $C^d A^L$. The distance between the two leaks are $0.46\lambda_{min}$ (left) and $0.23\lambda_{min}$ (right).

any measured frequencies generated by the transient wave. Fig. 9(b) displays the localization error where only resonant frequencies $\omega = \{(1+\alpha)\omega_{th} : \alpha = 0, 2, 4, \ldots, 30\}$ are used. In this case, the localization error is obviously higher than the previous case since less information from the measurement is used, which can also be inferred from the higher CRLB. The RMSE of leak size estimation is also shown in Fig. 9(c) and (d). Similar to the leak location estimation, in those cases having a leak distance greater than $0.15\lambda_{min}$ and for which frequencies $\omega = \{(1+\alpha)\omega_{th} : \alpha = 0, 0.02, 0.04, \ldots, 30\}$ are used, the estimation error is acceptable for all the SNRs. However, the estimation error using only resonant frequencies is larger than when using more frequencies, since less information is used in the parameter estimation. Furthermore, the RMSE of the leak size estimate is relatively further away from the corresponding CRLB than the leak location estimate. One possible reason is that the proposed ML approach independently estimates the leak location first and then uses the result of the first step to decide the leak size, therefore the error in the first step is possibly magnified in the second step.

It is somewhat remarkable that a large error of leak localization or size estimation does not always mean a useless result. Fig. 10 shows two leak identification results (with two specific realizations of random error) that plot leak location and size estimates, wherein SNR = −3 dB and leak distance is $0.08\lambda_{min}$. In both cases, the L_2-error of leak localization computed from Eq. (41) is respectively 110 m and 526 m, the relative error (RE) of leak size estimation computed from

$$RE(\hat{\mathbf{s}}^L) = \frac{1}{60}\sum_{n=1}^{30}\sqrt{\left[\left(\frac{\hat{s}_n^{L_1} - s^{L_1}}{s^{L_1}}\right)^2 + \left(\frac{\hat{s}_n^{L_2} - s^{L_2}}{s^{L_2}}\right)^2\right]} \tag{42}$$

is respectively 82% and 100%. However, in both figures one leak estimate with high amplitude locates between the two actual leaks (represented by the crosses) and the other leak estimate has a low amplitude and thus can be neglected. This result implies that the two leaks are not separated (i.e., a poor resolution) but replaced by a large leak estimate (the estimated size is approximately equal to the sum of the sizes of the two actual leaks) in between.

Finally, in order to justify the leak detection accuracy due to the model linearization Eq. (3), the localization error with respect to various leak size is investigated. The result is shown in Fig. 11 for leak distance equal to $0.46\lambda_{min}$ ($x^{L_1} = 400$ m and $x^{L_2} = 520$ m) and $0.23\lambda_{min}$ ($x^{L_1} = 400$ m and $x^{L_2} = 460$ m). The SNR is set to be relatively large, being 30 dB, to ignore the influence of random error. For realistic leak sizes the localization error is always acceptable; even for a very large size $C^d A^L \leqslant 2 \times 10^{-3}$ m^2 (the relative leak size is $C^d A^{L_1}/A = 1 \times 10^{-2}$) the L^2-error is less than 5 m for both cases. It is interesting that in the case of shorter distance ($0.23\lambda_{min}$) between the two leaks, the localization error is larger, although the modeling error due to linearization is smaller (cf. the dash line and the solid line in Fig. 4), which implies that a shorter leak range leads to a more sensitive leak localization with respect to modeling error.

7. Conclusions

This paper proposes a maximum likelihood (ML) approach for identifying multiple leaks in a water-filled pipeline based on inverse transient wave theory. The key findings are summarized below.

- The analytical solution of the multi-leak problem involves nonlinear interaction terms between the various leaks. This paper shows analytically and numerically that these nonlinear terms are of the order of the leak sizes to the power two. Therefore, the leak-leak interaction terms are relatively small and thus negligible.
- The fact that the leak-leak interaction terms are negligible is then exploited in the formulation of a ML scheme that identifies leak locations and leak sizes separately and sequentially.
- It is found that the ML estimation scheme is highly efficient and robust with respect to noise. In addition, the ML method is a super-resolution leak localization scheme because its resolvable leak distance (approximately $0.15\lambda_{min}$ (λ_{min} is the minimum wavelength)) is below the Nyquist-Shannon sampling theorem limit ($0.5\lambda_{min}$).
- The Cramér-Rao lower bound (CRLB) is derived and used to show the efficiency of the ML estimates. The variance of the ML estimator approximates the CRLB proving that the ML scheme belongs to class of best unbiased estimator of leak localization methods.
- The ML scheme maximizes the signal-to-noise ratio (SNR). In addition, it uses the full information in the measured signal (i.e., it uses all available frequencies, not just resonant frequencies).
- The fact that this class of schemes deals with noise and searches for leaks by maximizing the SNR is an important first step to applying TBDM to real-world systems in the field where noise from various sources (traffic, turbulence, mechanical devices, construction activities, etc) is ubiquitous.

Future work may be conducted in several directions. In real field application, the existence of uncertainties makes the leak detection more difficult. The current work provides a systematic framework for handling uncertainties when their distribution is known. In practice, the distribution of uncertainties that originate from lack of knowledge of system's topology and behavior of its devices, numerical and modeling errors, noise from traffic and other sources, and imprecise measurement of wave speed, friction factor and steady-state discharge is generally not known. Therefore, further progress requires efforts in studying the various uncertainties that could affect the leak detection. Furthermore, in the numerical examples in this paper, only the case of two-leak is considered, where the leak localization can be accomplished by plotting the two-dimensional likelihood function. In the case of high leak number, optimization problem has to be solved and other techniques are desired to decrease the computational complexity and cost. This issue is currently under development by the authors.

Acknowledgements

This work has been supported by research grants from the Research Grant Council of the Hong Kong SAR, China (Project No. T21-602/15R). The Chinese Estates are acknowledged for their support of this research. The authors would like to thank Duncan A. McInnis for discussion and editing.

Appendix A. Fisher information and Cramér-Rao lower bound

In the parameter estimation theory, Fisher information is a measure of information. More specifically, for a random variable X with PDF $p(x|\theta)$, the information of a sample of data that can provide about the unknown parameter θ is quantified by its Fisher information, which is defined by

$$I(\theta) = -\mathbb{E}\left(\frac{d^2 \log p(x|\theta)}{d\theta^2}\right) = -\int \frac{d^2 \log p(x|\theta)}{d\theta^2} p(x|\theta) dx. \tag{A.1}$$

Furthermore, this information determines the lower bound of the variance of an estimator of θ. If $\hat{\theta}$ is an unbiased estimator of θ, i.e., $\mathbb{E}(\hat{\theta}) = \theta$, then

$$\mathrm{Var}(\hat{\theta}) \geqslant \frac{1}{TI(\theta)}. \tag{A.2}$$

The right hand side of the above equation is known as CRLB.

For the case of multiple unknown parameters, denoted as $\Theta = (\theta_1, \ldots, \theta_N)$, the sample information is described by the Fisher information matrix (FIM):

$$\mathbf{I}(\Theta) = -\mathbb{E}\left(\frac{d^2 \log p(x|\Theta)}{d\Theta^2}\right) = -\left(\int \frac{d^2 \log p(x|\Theta)}{d\theta_{n_1} d\theta_{n_2}} p(x|\Theta) dx\right)_{n_1=1,n_2=1}^{N,N}. \tag{A.3}$$

Similarly, CRLB for the covariance matrix is obtained from FIM:

$$\mathrm{Cov}(\hat{\Theta}) \geqslant (T\mathbf{I}(\Theta))^{-1}. \tag{A.4}$$

Appendix B. Derivation of CRLB of leak location and size estimators

The log-likelihood function Eq. (24) is written as

$$\begin{aligned}\log L(\mathbf{x}^L, \mathbf{s}^L; \Delta\mathbf{h}) &= -JM \log(\pi\sigma^2) - \frac{1}{\sigma^2}\left\|\Delta\mathbf{h} - \sum_{n=1}^{N} \mathbf{G}_n(x^{L_n}) s^{L_n}\right\|^2 \\ &= -JM \log(\pi\sigma^2) - \frac{1}{\sigma^2}\left(\Delta\mathbf{h}^H \Delta\mathbf{h} - \Delta\mathbf{h}^H \sum_{n=1}^{N} \mathbf{G}_n s^{L_n} - \left(\sum_{n=1}^{N} \mathbf{G}_n s^{L_n}\right)^H \Delta\mathbf{h} + \sum_{n_1=1}^{N}\sum_{n_2=1}^{N} s^{L_{n_1}} s^{L_{n_2}} \mathbf{G}_{n_1}^H \mathbf{G}_{n_2}\right).\end{aligned} \tag{B.1}$$

If $n_1 \neq n_2$,

$$\frac{\partial^2 \log L}{\partial x^{L_{n_1}} \partial x^{L_{n_2}}} = -\frac{1}{\sigma^2} s^{L_{n_1}} s^{L_{n_2}} \left((\mathbf{G}'_{n_1})^H \mathbf{G}'_{n_2} + (\mathbf{G}'_{n_2})^H \mathbf{G}'_{n_1}\right) \tag{B.2}$$

and

$$\begin{aligned}\mathbb{E}\left(\frac{\partial^2 \log L}{\partial (x^{L_n})^2}\right) &= -\frac{1}{\sigma^2}\mathbb{E}\left(-\Delta\mathbf{h}^H \mathbf{G}''_n s^{L_n} - (\mathbf{G}''_n s^{L_n})^H \Delta\mathbf{h} + (\mathbf{s}^L)^H \frac{d^2 f(\mathbf{x}^L)}{d(x^{L_n})^2} \mathbf{s}^L\right) \\ &= -\frac{1}{\sigma^2}\left(-(\mathbf{G}\mathbf{s}^L)^H \mathbf{G}''_n s^{L_n} - (\mathbf{G}''_n s^{L_n})^H \mathbf{G}\mathbf{s}^L + s^{L_n} (\mathbf{G}''_n)^H \mathbf{G}\mathbf{s}^L + (\mathbf{s}^L)^H \mathbf{G}^H \mathbf{G}''_n s^{L_n} + 2|s^{L_n}|^2 \|\mathbf{G}'_n\|^2\right) \\ &= -\frac{2}{\sigma^2}|s^{L_n}|^2 \|\mathbf{G}'_n\|^2,\end{aligned} \tag{B.3}$$

therefore

$$\mathbb{E}\left(\frac{\partial^2 \log L}{\partial (\mathbf{x}^L)^2}\right) = -\frac{1}{\sigma^2} diag(\mathbf{s}^L)\left((\mathbf{G}')^H \mathbf{G}' + \left((\mathbf{G}')^H \mathbf{G}'\right)^\top\right) diag(\mathbf{s}^L), \tag{B.4}$$

in which $\mathbf{G}' = \left(\frac{d\mathbf{G}_1(x^{L_1})}{dx^{L_1}}, \ldots, \frac{d\mathbf{G}_N(x^{L_N})}{dx^{L_1}}\right)$ and $diag(\mathbf{s}^L)$ is a diagonal matrix with diagonal elements $s^{L_1}, \ldots, s^{L_N}$.

For any n_1 and n_2,

$$\frac{\partial^2 \log L}{\partial s^{L_{n_1}} \partial s^{L_{n_1}}} = -\frac{1}{\sigma^2}\left(\mathbf{G}_{n_1}^H \mathbf{G}_{n_2} + \mathbf{G}_{n_2}^H \mathbf{G}_{n_1}\right), \tag{B.5}$$

thus

$$\mathbb{E}\left(\frac{\partial^2 \log L}{\partial (\mathbf{s}^L)^2}\right) = -\frac{1}{\sigma^2}\left(\mathbf{G}^H\mathbf{G} + \left(\mathbf{G}^H\mathbf{G}\right)^\top\right), \tag{B.6}$$

If $n_1 \neq n_2$,

$$\frac{\partial^2 \log L}{\partial x^{L_{n_1}} \partial s^{L_{n_2}}} = -\frac{1}{\sigma^2} s^{L_{n_1}}\left((\mathbf{G}'_{n_1})^H \mathbf{G}_{n_2} + \mathbf{G}^H_{n_2}\mathbf{G}'_{n_1}\right), \tag{B.7}$$

and

$$\begin{aligned}\mathbb{E}\left(\frac{\partial^2 \log L}{\partial x^{L_n} \partial s^{L_n}}\right) &= -\frac{1}{\sigma^2}\mathbb{E}\left(-\Delta\mathbf{h}^H\mathbf{G}'_n - (\mathbf{G}'_n)^H\Delta\mathbf{h} + (\mathbf{G}'_n)^H\mathbf{G}\mathbf{s}^L + s^{L_n}(\mathbf{G}'_n)^H\mathbf{G}_n + \left(\mathbf{G}\mathbf{s}^L\right)^H\mathbf{G}'_n + s^{L_n}\mathbf{G}^H_n\mathbf{G}'_n\right)\\ &= -\frac{1}{\sigma^2} s^{L_n}\left((\mathbf{G}'_n)^H\mathbf{G}_n + \mathbf{G}^H_n\mathbf{G}'_n\right),\end{aligned} \tag{B.8}$$

therefore

$$\mathbb{E}\left(\frac{\partial^2 \log L}{\partial \mathbf{x}^L \partial \mathbf{s}^L}\right) = -\frac{1}{\sigma^2} diag(\mathbf{s}^L)\left((\mathbf{G}')^H\mathbf{G} + \left(\mathbf{G}^H\mathbf{G}'\right)^\top\right) \tag{B.9}$$

and

$$\mathbb{E}\left(\frac{\partial^2 \log L}{\partial \mathbf{s}^L \partial \mathbf{x}^L}\right) = -\frac{1}{\sigma^2}\left(\mathbf{G}^H\mathbf{G}' + \left((\mathbf{G}')^H\mathbf{G}\right)^\top\right) diag(\mathbf{s}^L). \tag{B.10}$$

Denote $\Theta = \{\mathbf{x}^L, \mathbf{s}^L\}$, by Eqs. (B.4), (B.6), (B.9), (B.10), the FIM is obtained:

$$\mathbf{I}(\Theta) = -\mathbb{E}\begin{pmatrix} \frac{\partial^2 \log L}{\partial (\mathbf{x}^L)^2} & \frac{\partial^2 \log L}{\partial \mathbf{x}^L \partial \mathbf{s}^L} \\ \frac{\partial^2 \log L}{\partial \mathbf{s}^L \partial \mathbf{x}^L} & \frac{\partial^2 \log L}{\partial (\mathbf{s}^L)^2} \end{pmatrix} = \frac{1}{\sigma^2}\begin{pmatrix} diag(\mathbf{s}^L) & \mathbf{0} \\ \mathbf{0} & \mathbf{I}_N \end{pmatrix}\begin{pmatrix} (\mathbf{G}')^H\mathbf{G}' + \left((\mathbf{G}')^H\mathbf{G}'\right)^\top & (\mathbf{G}')^H\mathbf{G} + \left(\mathbf{G}^H\mathbf{G}'\right)^\top \\ \mathbf{G}^H\mathbf{G}' + \left((\mathbf{G}')^H\mathbf{G}\right)^\top & \mathbf{G}^H\mathbf{G} + \left(\mathbf{G}^H\mathbf{G}\right)^\top \end{pmatrix}\begin{pmatrix} diag(\mathbf{s}^L) & \mathbf{0} \\ \mathbf{0} & \mathbf{I}_N \end{pmatrix}. \tag{B.11}$$

Thus, the CRLB of Θ estimator reduces to

$$CRLB(\hat{\Theta}) = (T\mathbf{I}(\Theta))^{-1}. \tag{B.12}$$

Here, $\mathbf{G}'_n(x^{L_n})$ is obtained from the derivative of Eqs. (20) and (15). Assume that $z_0^{L_n} = 0$, i.e., the pipe is in the same horizontal plane, and $H_0^{L_n} = H^U + (H^D - H^U)x^{L_n}/l$, then each entry of $\mathbf{G}'_n(x^{L_n})$ is

$$\frac{G(\omega_j, x^{L_n}, x_m)}{dx^{L_n}} = \frac{\sqrt{g}Z^2 q(x^U)}{\sqrt{2H_0^{L_n}}}\sinh\left(\mu(x_m - 2x^{L_n})\right)\left(-\mu + \frac{H^D - H^U}{4lH_0^{L_n}}\sinh\left(\mu x^{L_n}\right)\right). \tag{B.13}$$

Appendix C. Derivation of leak size estimate of MFP

The proof of Eq. (34) is given here. Denote

$$\mathbf{v} = \mathbf{G}(\mathbf{x}^L)\mathbf{s}^L, \tag{C.1}$$

where $\mathbf{G}$ is an $MJ \times N$ matrix. Assuming that $MJ > N$, then the left pseudo inverse of $\mathbf{G}$ is

$$\mathbf{G}^{-1}_{left} = \left(\mathbf{G}^H\mathbf{G}\right)^{-1}\mathbf{G}^H, \tag{C.2}$$

thus

$$\mathbf{s}^L = \mathbf{G}^{-1}_{left}\mathbf{v} = \left(\mathbf{G}^H\mathbf{G}\right)^{-1}\mathbf{G}^H\mathbf{v}. \tag{C.3}$$

For any fixed $\mathbf{x}^L$, the optimal $\mathbf{s}^L$ is obtained by inserting Eqs. (C.1) and (C.3) into the denominator and numerator of Eq. (33) and maximizing it:

$$\hat{\mathbf{s}}^L = \arg\max_{\mathbf{s}^L} \frac{\left|\Delta\mathbf{h}^H\mathbf{G}\mathbf{s}^L\right|^2}{\left\|\mathbf{G}\mathbf{s}^L\right\|^2} = \arg\max_{\mathbf{s}^L} \frac{\left|\Delta\mathbf{h}^H\mathbf{G}(\mathbf{G}^H\mathbf{G})^{-1}\mathbf{G}^H\mathbf{v}\right|^2}{\|\mathbf{v}\|^2} = \arg\max_{\mathbf{s}^L} \left|\left\langle \mathbf{G}(\mathbf{G}^H\mathbf{G})^{-1}\mathbf{G}^H\Delta\mathbf{h}, \frac{\mathbf{v}}{\|\mathbf{v}\|}\right\rangle\right|^2$$
$$= \arg\max_{\mathbf{s}^L} \left|\left\langle \mathbf{G}(\mathbf{G}^H\mathbf{G})^{-1}\mathbf{G}^H\Delta\mathbf{h}, \frac{\mathbf{G}\mathbf{s}^L}{\left\|\mathbf{G}\mathbf{s}^L\right\|}\right\rangle\right|^2 = \left(\mathbf{G}^H\mathbf{G}\right)^{-1}\mathbf{G}^H\Delta\mathbf{h}. \tag{C.4}$$

The last equality holds due to Cauchy-Schwarz inequality and $\langle\cdot,\cdot\rangle$ stands for inner product.

References

[1] J.A. Liggett, L.-C. Chen, Inverse transient analysis in pipe networks, J. Hydraulic Eng. 120 (8) (1994) 934–955.
[2] B. Brunone, Transient test-based technique for leak detection in outfall pipes, J. Water Resources Plann. Manage. 125 (5) (1999) 302–306.
[3] J.P. Vítkovskỳ, A.R. Simpson, M.F. Lambert, Leak detection and calibration using transients and genetic algorithms, J. Water Resources Plann. Manage. 126 (4) (2000) 262–265.
[4] W. Mpesha, S.L. Gassman, M.H. Chaudhry, Leak detection in pipes by frequency response method, J. Hydraul. Eng. 127 (2) (2001) 134–147.
[5] X.-J. Wang, M.F. Lambert, A.R. Simpson, J.A. Liggett, J.P. Vítkovskỳ, Leak detection in pipelines using the damping of fluid transients, J. Hydraul. Eng. 128 (7) (2002) 697–711.
[6] P.J. Lee, J.P. Vitkovsky, M.F. Lambert, A.R. Simpson, J.A. Liggett, Frequency response coding for the location of leaks in single pipeline systems, in: The Int. Conference on Pumps, Electromechanical Devices and Systems Applied to Urban Water Management, IAHR and IHRA, Valencia, Spain, April 22–25, 2003.
[7] P.J. Lee, J.P. Vítkovskỳ, M.F. Lambert, A.R. Simpson, J.A. Liggett, Frequency domain analysis for detecting pipeline leaks, J. Hydraul. Eng. 131 (7) (2005) 596–604.
[8] P.J. Lee, J.P. Vítkovskỳ, M.F. Lambert, A.R. Simpson, J.A. Liggett, Leak location using the pattern of the frequency response diagram in pipelines: a numerical study, J. Sound Vib. 284 (3) (2005) 1051–1073.
[9] P.J. Lee, M.F. Lambert, A.R. Simpson, J.P. Vítkovskỳ, J. Liggett, Experimental verification of the frequency response method for pipeline leak detection, J. Hydraul. Res. 44 (5) (2006) 693–707.
[10] H.-F. Duan, P.J. Lee, M.S. Ghidaoui, Y.-K. Tung, Essential system response information for transient-based leak detection methods, J. Hydraul. Res. 48 (5) (2010) 650–657.
[11] H.-F. Duan, P.J. Lee, M.S. Ghidaoui, Y.-K. Tung, Leak detection in complex series pipelines by using the system frequency response method, J. Hydraul. Res. 49 (2) (2011) 213–221.
[12] H.-F. Duan, P.J. Lee, M.S. Ghidaoui, Y.-K. Tung, System response function–based leak detection in viscoelastic pipelines, J. Hydraul. Eng. 138 (2) (2011) 143–153.
[13] W. Nixon, M.S. Ghidaoui, Numerical sensitivity study of unsteady friction in simple systems with external flows, J. Hydraul. Eng. 133 (7) (2007) 736–749.
[14] M.F. Ghazali, S.B.M. Beck, J.D. Shucksmith, J.B. Boxall, W.J. Staszewski, Comparative study of instantaneous frequency based methods for leak detection in pipeline networks, Mech. Syst. Signal Process. 29 (2012) 187–200.
[15] A.C. Zecchin, L.B. White, M.F. Lambert, A.R. Simpson, Parameter identification of fluid line networks by frequency-domain maximum likelihood estimation, Mech. Syst. Signal Process. 37 (1) (2013) 370–387.
[16] S. Meniconi, B. Brunone, M. Ferrante, C. Capponi, C.A. Carrettini, C. Chiesa, D. Segalini, E.A. Lanfranchi, Anomaly pre-localization in distribution–transmission mains by pump trip: preliminary field tests in the milan pipe system, J. Hydroinformat. 17 (3) (2015) 377–389.
[17] S. Meniconi, B. Brunone, M. Ferrante, C. Massari, Potential of transient tests to diagnose real supply pipe systems: what can be done with a single extemporary test, J. Water Resources Plann. Manage. 137 (2) (2010) 238–241.
[18] M.L. Stephens, M.F. Lambert, A.R. Simpson, J.P. Vitkovsky, Calibrating the water-hammer response of a field pipe network by using a mechanical damping model, J. Hydraul. Eng. 137 (10) (2011) 1225–1237.
[19] K.W. Tang, B. Brunone, B. Karney, A. Rossetti, Role and characterization of leaks under transient conditions, in: Building Partnerships-Proc. ASCE Joint Conf. Water Resource Engineering and Management Minneapolis MN, 7–30, 2000.
[20] B. Brunone, M. Ferrante, Detecting leaks in pressurised pipes by means of transients, J. Hydraul. Res. 39 (5) (2001) 539–547.
[21] D. Covas, H. Ramos, N. Graham, C. Maksimovic, Application of hydraulic transients for leak detection in water supply systems, Water Sci. Technol.: Water Supp. 4 (5–6) (2005) 365–374.
[22] M. Ferrante, B. Brunone, S. Meniconi, Wavelets for the analysis of transient pressure signals for leak detection, J. Hydraul. Eng. 133 (11) (2007) 1274–1282.
[23] S.T.N. Nguyen, J. Gong, M.F. Lambert, A.C. Zecchin, A.R. Simpson, Least squares deconvolution for leak detection with a pseudo random binary sequence excitation, Mech. Syst. Signal Process. 99 (2018) 846–858.
[24] J.C. Liou, Pipeline leak detection by impulse response extraction, J. Fluids Eng. 120 (4) (1998) 833–838.
[25] M. Ferrante, B. Brunone, Pipe system diagnosis and leak detection by unsteady-state tests. I. Harmonic analysis, Adv. Water Resources 26 (1) (2003) 95–105.
[26] D. Covas, H. Ramos, A.B. De Almeida, Standing wave difference method for leak detection in pipeline systems, J. Hydraul. Eng. 131 (12) (2005) 1106–1116.
[27] A.M. Sattar, M.H. Chaudhry, Leak detection in pipelines by frequency response method, J. Hydraul. Res. 46 (EI1) (2008) 138–151.
[28] M. Taghvaei, S.B.M. Beck, J.B. Boxall, Leak detection in pipes using induced water hammer pulses and cepstrum analysis, Int. J. COMADEM 13 (1) (2010) 19.
[29] M.L. Stephens, Transient response analysis for fault detection and pipeline wall condition assessment in field water transmission and distribution pipelines and networks (Ph.D. thesis), University of Adelaide, 2008.
[30] D. Covas, H. Ramos, Case studies of leak detection and location in water pipe systems by inverse transient analysis, J. Water Resources Plann. Manage. 136 (2) (2010) 248–257.
[31] S. Meniconi, H.F. Duan, P.J. Lee, B. Brunone, M.S. Ghidaoui, M. Ferrante, Experimental investigation of coupled frequency and time-domain transient test–based techniques for partial blockage detection in pipelines, J. Hydraul. Eng. 139 (10) (2013) 1033–1040.
[32] I. Rubio Scola, G. Besançon, D. Georges, Blockage and leak detection and location in pipelines using frequency response optimization, J. Hydraul. Eng. 143 (1) (2016) 04016074.
[33] S. Meniconi, B. Brunone, M. Ferrante, C. Massari, Transient hydrodynamics of in-line valves in viscoelastic pressurized pipes: long-period analysis, Exp. Fluids 53 (1) (2012) 265–275.
[34] X. Wang, M.S. Ghidaoui, Pipeline leak detection using the matched-field processing method, J. Hydraul. Eng. (2008), https://doi.org/10.1061/(ASCE)HY.1943-7900.0001476.
[35] M.H. Chaudhry, Applied Hydraulic Transients, third ed., Springer, 2014.

[36] A. Kashima, P. J Lee, R. Nokes, Numerical errors in discharge measurements using the KDP method, J. Hydraul. Res. 50 (1) (2012) 98–104.
[37] A. Kashima, P.J. Lee, M.S. Ghidaoui, M. Davidson, Experimental verification of the kinetic differential pressure method for flow measurements, J. Hydraul. Res. 51 (6) (2013) 634–644.
[38] S.M. Kay, Fundamentals of statistical signal processing, volume I: estimation theory, 1993.
[39] H. Krim, M. Viberg, Two decades of array signal processing research, IEEE Signal Process. Mag. 13 (4) (1996) 67–94.
[40] A.B. Baggeroer, W.A. Kuperman, P.N. Mikhalevsky, An overview of matched field methods in ocean acoustics, IEEE J. Oceanic Eng. 18 (4) (1993) 401–424.
[41] X. Wang, B. Quost, J.-D. Chazot, J. Antoni, Estimation of multiple sound sources with data and model uncertainties using the EM and evidential EM algorithms, Mech. Syst. Signal Process. 66–67 (2016) 159–177.
[42] X. Wang, B. Quost, J.-D. Chazot, J. Antoni, Iterative beamforming for identification of multiple broadband sound sources, J. Sound Vib. 365 (2016) 260–275.
[43] M. Ferrante, B. Brunone, S. Meniconi, B.W. Karney, C. Massari, Leak size, detectability and test conditions in pressurized pipe systems, Water Resources Manage. 28 (13) (2014) 4583–4598.